Metal-Catalyzed Multi-Component Approach to Quinoline-Linked Covalent Organic Frameworks

Xianghao Han[a]
Shuda Dong[a]
Xiao Feng[*] [a]

[a] Beijing Key Laboratory of Photoelectronic/Electrophotonic Conversion Materials, Key Laboratory of Cluster Science, Ministry of Education, Advanced Technology Research Institute (Jinan), Frontiers Science Center for High Energy Material, School of Chemistry and Chemical Engineering, Beijing Institute of Technology. No. 5, South Street, Zhongguancun, Haidian District, Beijing 100081, P. R. of China

[*] fengxiao86@bit.edu.cn

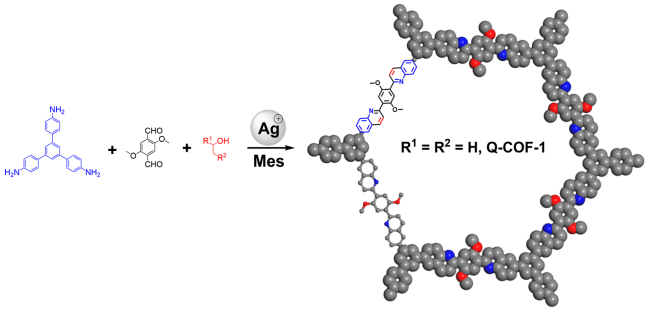

Received: 01.02.2024
Accepted after revision: 18.04.2024
DOI: 10.1055/s-0044-1787016; Art ID: OM-2024-02-0003-SC

Abstract The development of new reaction chemistry is highly desirable to construct new structural and functional covalent organic frameworks (COFs). Benefiting from the extremely large database of metal-catalyzed reaction database, we herein develop a new synthetic strategy that can generate quinoline-linked COFs via a silver-catalyzed three-component one-pot reaction and achieve functionalization by the simple replacement of alcohols. This metal-catalyzed approach to the construction of robust COF structures characterized by extended π-conjugation holds the potential to pave a novel pathway in the synthesis of COF materials endowed with both heightened stability and functionality.

Key words: covalent organic frameworks, silver-catalyzed, three-component, one-pot, quinoline-linked

Introduction

Covalent organic frameworks (COFs) are an emerging class of crystalline porous materials featuring periodic structures.[1–4] Owing to their designable structures and tailored functionalities, COFs have shown great potential in broad fields including gas storage and separation,[5,6] catalysis,[7–12] sensing,[13–17] drug delivery,[18–21] energy storage,[22–24] and so on. Since the first two COFs were reported by Yaghi in 2005,[25] progress in organic chemistry has shown significant contributions to the construction of COFs,[26,27] and their formation mechanisms have been deeply explored.[28–31] The formation of periodic COF frameworks is guided by the principles of dynamic covalent chemistry, in which the final products are determined by their thermodynamic equilibrium.[32,33] Nevertheless, this intrinsic reversibility concurrently imparts inherent instability to the resultant frameworks. To develop novel COFs and/or customize their functionality, researchers have undertaken the assembly of periodic COF frameworks using irreversible reactions, resulting in significant and noteworthy advancements. For instance, a variety of synthetic strategies, including the direct synthesis method, reversible covalent bond-based tandem reactions, post-synthetic modification, and multicomponent reactions, are used for building polyimide COFs,[18,34–37] olefin-linked COFs,[38–42] dioxin-linked COFs,[43–45] and many others.[46–51] As we all know, metal-catalyzed reaction chemistry, a crucially important part of chemistry, has found extensive applications in organic synthesis, industrial production, and biomedicine.[52,53] At present, COF materials are mainly used as carriers of active metal centers to carry out catalytic reactions of small molecules. It is noteworthy that there are currently few reports regarding the synthesis of COF materials through metal-catalyzed irreversible reactions.[54] This scarcity can be attributed primarily to the near insolubility of porous materials, which significantly hampers the advancement of reactions and the expansion of frameworks. Consequently, the utilization of metal-catalyzed reactions to achieve high crystallinity and porosity COF materials with new structures and new functions is of great significance. Herein, we introduce the metal-catalyzed reaction to synthesize COF materials.

This report was inspired by a silver-catalyzed three-component approach to quinolines starting from anilines, aldehydes, and alcohols (Scheme 1a).[55] Building upon this foundation, we have advanced a silver-catalyzed three-component one-pot approach, including Schiff's base reaction to construct the COF backbone followed by the key silver-catalyzed sequential process for the formation of two carbon–carbon (C–C) bonds, gradually constructing COF materials based on multi-substituted quinolines (Figure S1). Specifically, our investigation focuses on the reaction involving 1,3,5-tris(4-aminophenyl)benzene (TAPB) paired with 2,5-

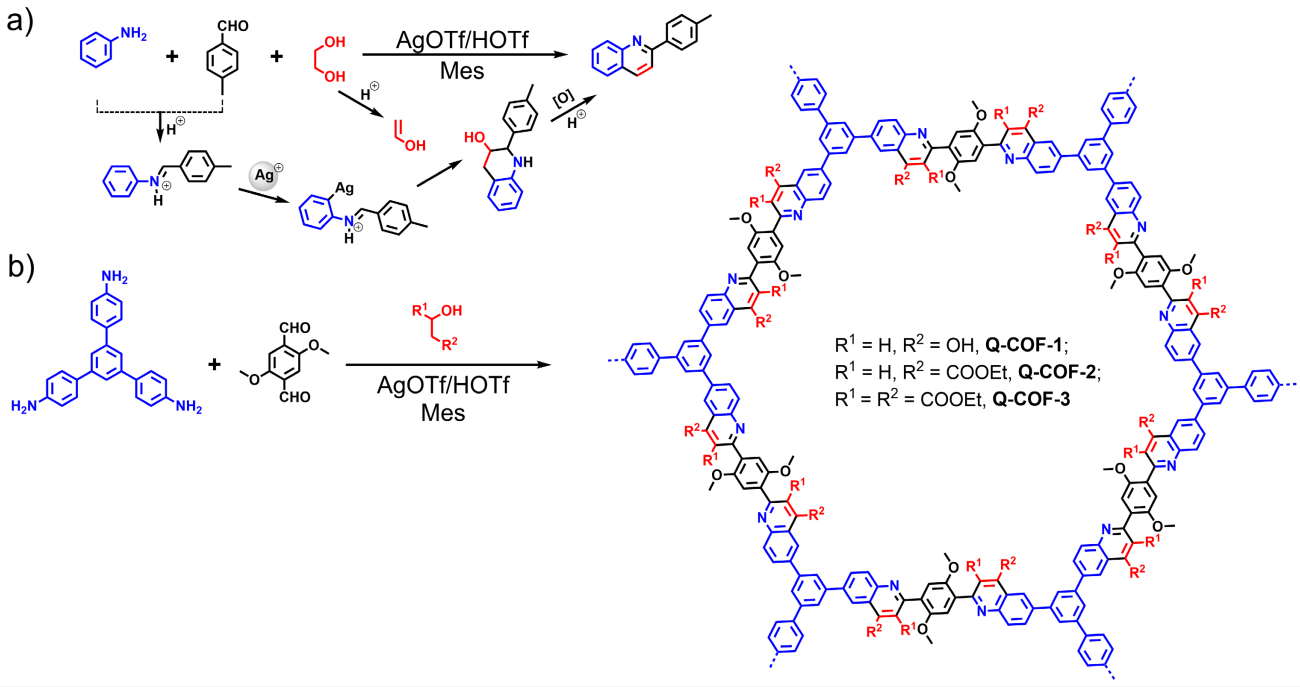

Scheme 1 a) Synthesis of model molecule. b) Synthesis of Q-COF-1, -2, and -3.

dimethoxyterephthalaldehyde (DMTP), alongside various alcohols (namely, ethylene glycol, ethyl lactate ester, and L-diethyl malate), in the presence of silver trifluoromethanesulfonate (AgOTf) and trifluoromethanesulfonic acid (HOTf) to yield polysubstituted quinoline-linked periodic frameworks (Scheme 1b). The silver-catalyzed three-component reaction was performed in mesitylene, sealed in an atmospheric atmosphere, and then heated at 120 °C without disturbance for 24 h. Crystalline solids of quinoline-linked COFs (Q-COF-1, -2, and -3) were obtained with isolated yields of 98 %,[56] 56 %, and 61 %, respectively (see the Supporting Information for details).

Results and Discussion

To confirm the structure of the obtained materials, we synthesized COF-1 in mesitylene for comparison (see the Supporting Information for details).[57] The formation of quinoline-linked Q-COFs (Q-COF-1, -2, and -3) was initially assessed by Fourier transform infrared spectroscopy. As shown in Figures S2 – S4, the disappearance of C(=O)–H (2869 and 2759 cm^{-1} of DMTP), N–H (3496 – 3326 cm^{-1} of TAPB) and O–H (3420 – 3345 cm^{-1}) vibration indicated a high degree of polymerization by consuming almost all the aldehyde, amine, and alcohol groups of the monomers. In addition, the appearance of absorption bands around 1615 cm^{-1} suggests the formation of C=N bonds by a Schiff's base reaction, together with a weak peak around 1642, 1558, and 1238 cm^{-1}, indicating the existence of a quinoline moiety (Figure S5). Furthermore, the appearance of absorption bands of *C*(OMe)=*O* at 1676 and 1678 cm^{-1} further supports the formation of a quinoline moiety (Figures S3 and S4). Solid-state ^{13}C cross-polarization magic-angle-spinning nuclear magnetic resonance (CP/MAS NMR) spectra of Q-COFs further supports the formation of quinoline units (Figures S6 – S8). The existence of carbon peaks at 154, 154, and 153 ppm was observed, which could be attributed to C=N bonds of quinoline for Q-COF-1, Q-COF-2, and Q-COF-3, respectively. In contrast to Q-COF-1 (Figure S6), the presence of distinct carbon peaks at 180, 53, and 18 ppm, associated with *C*(O)CH_2CH_3, C(O)*C*H_2CH_3, and C(O)CH_2*C*H_3 respectively, substantiates the synthesis of functionalized Q-COF-2 through the utilization of ethyl lactate ester (Figure S7). For Q-COF-3, comparable carbon peaks resembling those found in Q-COF-2 were identified. Nonetheless, a notable divergence is observed with the emergence of an enveloped peak at 55 ppm, attributed to the C(O)CH_2CH_3 and OCH_3 functionalities originating from L-diethyl malate and DMTP, respectively. Additionally, there is a discernible enhancement in the methyl signal corresponding to C(O)CH_2CH_3 (Figure S8). X-ray photoelectron spectroscopy analyses provided additional validation for the above results. Specifically, the N1s peak was detected at 401.13, 401.22, and 400.99 eV, corresponding to the N1s of C=N bonds within quinoline moieties.[49,58] This observation unequivocally confirms the suc-

cessful formation of quinoline units (Figures S9–S11). Field emission scanning electron microscopy and transmission electron microscopy show that Q-COF-1 exhibits a rod-shaped morphology (Figures S12 and S13), Q-COF-2 adopts a nanoparticle morphology (Figures S14 and S15), and Q-COF-3 displays a flake aggregation morphology (Figures S16 and S17).

In addition, the crystal structures of these samples were elucidated utilizing powder X-ray diffraction (PXRD), employing comparison with optimized, idealized structural models of the expected frameworks. As anticipated, the diffraction patterns of the three structurally analogous frameworks exhibit comparable characteristic reflections (Figure 1a). The PXRD pattern, as depicted in Figure 1, illustrates a series of prominent peaks at $2\theta = 2.67°$ (100), 4.80° (110), 5.56° (200), and 7.40° (210) for Q-COF-1; $2\theta = 2.68°$ (100), 4.72° (110), 5.47° (200), and 7.27° (210) for Q-COF-2; and $2\theta = 2.67°$ (100), 4.74° (110), 5.46° (200), and 7.29° (210) for Q-COF-3. Lattice modeling and Pawley refinement were conducted using Materials Studio software to generate their probable structures characterized by 2D AA stacking and AB stacking. The comparison between the experimental PXRD patterns and the simulated ones indicates a closer alignment of the experimental diffraction peaks (Figure 1, black) with the simulated patterns exhibiting AA stacking (Figure 1, orange) better than those featuring AB stacking (Figure 1, purple). The difference plots (Figure 1, gray) suggest that the refined PXRD patterns (Figure 1, red dot) are consistent with the experimental ones. Pawley refinements were conducted to determine the unit cell parameters. For Q-COF-1, the refined parameters were found to be $a = b = 37.07$ Å, $c = 3.94$ Å, $\alpha = \beta = 90°$, and $\gamma = 120°$, yielding residuals $R_p = 4.26\%$ and $R_{wp} = 5.33\%$ (Tables S1 and S4). Similarly, for Q-COF-2, the parameters were determined as $a = b = 36.97$ Å, $c = 4.10$ Å, $\alpha = \beta = 90°$, and $\gamma = 120°$, resulting in residuals $R_p = 5.33\%$ and $R_{wp} = 7.03\%$ (Tables S2 and S5). Lastly, for Q-COF-3, the refined parameters were $a = b = 36.93$ Å, $c = 4.82$ Å, $\alpha = \beta = 90°$, and $\gamma = 120°$, with residuals $R_p = 3.59\%$ and $R_{wp} = 4.48\%$ (Tables S3 and S6). These values closely approximate the corresponding structural models, further confirming that the successful synthesis of Q-COFs adopts AA stacking consistent with COF-1.

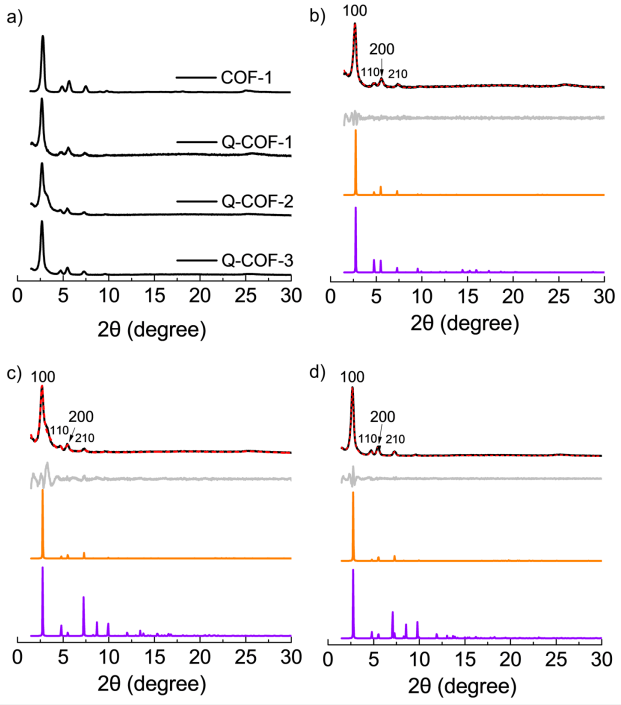

Figure 1 a) Experimental PXRD patterns of COF-1, Q-COF-1, Q-COF-2, and Q-COF-3. Experimental (black), Pawley-refined (red) PXRD patterns, difference plot between the observed and refined patterns (light grey), AA stacking patterns (orange), and AB stacking patterns (purple) for b) Q-COF-1, c) Q-COF-2, and d) Q-COF-3.

To assess their permanent porosity, nitrogen sorption measurements of COF-1 and Q-COFs were further carried out at 77 K. As shown in Figure 2, This sorption profile of Q-COFs and COF-1 is best described as a type IV isotherm with rapid N_2 uptakes at the low relative pressure range $P/P_0 < 0.05$, which is characteristic of mesoporous materials. Their Brunauer–Emmett–Teller (BET) surface areas were calculated to be 2200, 1123, 1261, and 1245 m^2/g (Figure S18), with total pore volumes (at $P/P_0 = 0.99$) being 2.116, 0.855, 0.812, and 0.933 cm^3/g for COF-1, Q-COF-1, Q-COF-2, and Q-COF-3, respectively. In comparison, the BET surface areas and pore volume of the Q-COFs synthesized via the silver-catalyzed multicomponent one-pot reaction are notably lower than those of the reference COF-1. Their pore size distributions (PSDs) of Q-COFs and COF-1 calculated by quenched solid functional theory were evaluated to be

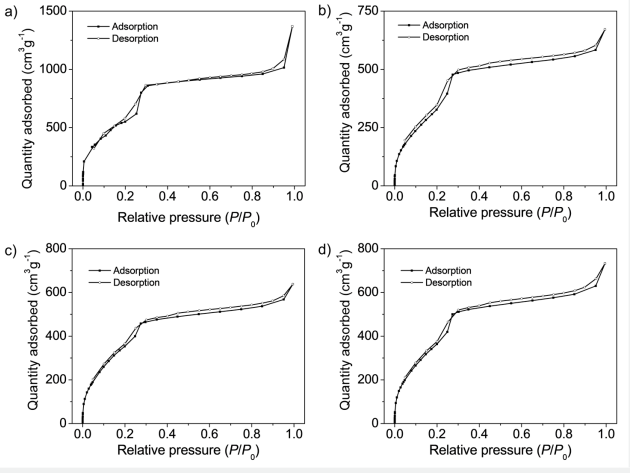

Figure 2 N_2 sorption isotherm curves of a) COF-1, b) Q-COF-1, c) Q-COF-2, and d) Q-COF-3.

3.43 nm for COF-1, 3.30 nm for Q-COF-1, and 2.89 nm for Q-COF-2 and Q-COF-3, respectively (Figure S19). For COF-1 and Q-COF-1, their PSD corresponded well with previously reported findings.[57] In the case of Q-COF-2 and Q-COF-3, their PSD aligned closely with the theoretical pore diameter associated with their eclipsed (AA) layer stacking configuration (2.52 nm for Q-COF-2 and 2.41 nm for Q-COF-3, Figure S20). Other minor peak distributions indicate the existence of defects in the obtained COFs.

The thermal stability of Q-COFs was assessed utilizing a thermogravimetric analyzer under a nitrogen atmosphere. As illustrated in Figure S21, for Q-COF-1, the temperature reached approximately 252 °C, resulting in a thermal weight loss proportion of approximately 1.5%, with the temperature corresponding to a 5% thermal weight loss recorded at 313 °C. Similarly, for Q-COF-2, the temperature reached around 264 °C, accompanied by a thermal weight loss proportion of approximately 1.5%, and a corresponding temperature for a 5% thermal weight loss recorded at 343 °C. For Q-COF-3, the temperature reached approximately 262 °C, resulting in a thermal weight loss proportion of approximately 1.5%, with the temperature corresponding to a 5% thermal weight loss recorded at 307 °C. These findings indicate the favorable thermal stability properties of Q-COFs.

Conclusions

In summary, we have presented an efficient method for fabricating stable, crystalline, porous quinoline-linked COFs. This multi-component reaction involves readily available aldehydes, amines, and alcohols in a one-pot process via a silver-catalyzed cyclization reaction. Furthermore, the functionalization of frameworks is achieved through the direct substitution of alcohols. We anticipate that this strategy will provide a versatile and feasible method for constructing numerous novel COF materials and will be adopted by others and used to explore further material applications, possibly greatly expanding the family of COF materials.

Funding Information

This work was supported in part by the National Natural Science Foundation of China (Grant Nos. 21922502, 22171022, 21971017), the Natural Science Foundation of Shandong Province (Grant No. ZR2021QB170), China Postdoctoral Science Foundation (Grant No. 2021M700416), and Beijing Municipal Science and Technology Commission (No. Z211100002421013).

Supporting Information

Supporting Information for this article is available online at https://doi.org/10.1055/s-0044-1787016.

Conflict of Interest

The authors declare no conflict of interest.

References and Notes

(1) El-Kaderi, H. M.; Hunt, J. R.; Mendoza-Cortes, J. L.; Cote, A. P.; Taylor, R. E.; O'Keeffe, M.; Yaghi, O. M. *Science* **2007**, *316*, 268.
(2) Waller, P. J.; Gandara, F.; Yaghi, O. M. *Acc. Chem. Res.* **2015**, *48*, 3053.
(3) Liu, R.; Tan, K. T.; Gong, Y.; Chen, Y.; Li, Z.; Xie, S.; He, T.; Lu, Z.; Yang, H.; Jiang, D. *Chem. Soc. Rev.* **2021**, *50*, 120.
(4) Lohse, M. S.; Bein, T. *Adv. Funct. Mater.* **2018**, *28*, 1705553.
(5) Han, S. S.; Furukawa, H.; Yaghi, O. M.; Goddard, W. A. *J. Am. Chem. Soc.* **2008**, *130*, 11580.
(6) Huang, N.; Chen, X.; Krishna, R.; Jiang, D. *Angew. Chem. Int. Ed.* **2015**, *54*, 2986.
(7) Ding, S.-Y.; Gao, J.; Wang, Q.; Zhang, Y.; Song, W.-G.; Su, C.-Y.; Wang, W. *J. Am. Chem. Soc.* **2011**, *133*, 19816.
(8) Wang, X.; Han, X.; Zhang, J.; Wu, X.; Liu, Y.; Cui, Y. *J. Am. Chem. Soc.* **2016**, *138*, 12332.
(9) Guo, J.; Jiang, D. *ACS Cent. Sci.* **2020**, *6*, 869.
(10) Liu, J.; Wang, N.; Ma, L. *Chem. Asian J.* **2020**, *15*, 338.
(11) Jati, A.; Dey, K.; Nurhuda, M.; Addicoat, M. A.; Banerjee, R.; Maji, B. *J. Am. Chem. Soc.* **2022**, *144*, 7822.
(12) Vyas, V. S.; Haase, F.; Stegbauer, L.; Savasci, G.; Podjaski, F.; Ochsenfeld, C.; Lotsch, B. V. *Nat. Commun.* **2015**, *6*, 8508.
(13) Zhang, J. L.; Yao, L. Y.; Yang, Y.; Liang, W. B.; Yuan, R.; Xiao, D. R. *Anal. Chem.* **2022**, *94*, 3685.
(14) Yao, D.; Li, C.; Wang, H.; Wen, G.; Liang, A.; Jiang, Z. *Sens. Actuators, B* **2020**, *319*, 128308.
(15) Li, Y.; Chen, M.; Han, Y.; Feng, Y.; Zhang, Z.; Zhang, B. *Chem. Mater.* **2020**, *32*, 2532.
(16) Cui, F.-Z.; Xie, J.-J.; Jiang, S.-Y.; Gan, S.-X.; Ma, D.-L.; Liang, R.-R.; Jiang, G.-F.; Zhao, X. *Chem. Commun.* **2019**, *55*, 4550.
(17) Li, Z.; Zhang, Y.; Xia, H.; Mu, Y.; Liu, X. *Chem. Commun.* **2016**, *52*, 6613.
(18) Fang, Q.; Wang, J.; Gu, S.; Kaspar, R. B.; Zhuang, Z.; Zheng, J.; Guo, H.; Qiu, S.; Yan, Y. *J. Am. Chem. Soc.* **2015**, *137*, 8352.
(19) Mitra, S.; Sasmal, H. S.; Kundu, T.; Kandambeth, S.; Illath, K.; Diaz Diaz, D.; Banerjee, R. *J. Am. Chem. Soc.* **2017**, *139*, 4513.
(20) Das, S.; Sekine, T.; Mabuchi, H.; Irie, T.; Sakai, J.; Zhao, Y.; Fang, Q.; Negishi, Y. *ACS Appl. Mater. Interfaces* **2022**, *14*, 48045.
(21) Du, C.; Na, W.; Shao, M.; Shang, S.; Liu, Y.; Chen, J. *Chem. Mater.* **2023**, *35*, 1395.
(22) DeBlase, C. R.; Silberstein, K. E.; Thanh-Tam, T.; Abruna, H. D.; Dichtel, W. R. *J. Am. Chem. Soc.* **2013**, *135*, 16821.
(23) Xu, F.; Xu, H.; Chen, X.; Wu, D.; Wu, Y.; Liu, H.; Gu, C.; Fu, R.; Jiang, D. *Angew. Chem. Int. Ed.* **2015**, *54*, 6814.
(24) Li, J.; Jing, X.; Li, Q.; Li, S.; Gao, X.; Feng, X.; Wang, B. *Chem. Soc. Rev.* **2020**, *49*, 3565.
(25) Côté, A. P.; Benin, A. I.; Ockwig, N. W.; O'Keeffe, M.; Matzger, A. J.; Yaghi, O. M. *Science* **2005**, *310*, 1166.

(26) Keller, N.; Bein, T. *Chem. Soc. Rev.* **2021**, *50*, 1813.
(27) Su, Y.; Li, B.; Xu, H.; Lu, C.; Wang, S.; Chen, B.; Wang, Z.; Wang, W.; Otake, K. I.; Kitagawa, S.; Huang, L.; Gu, C. *J. Am. Chem. Soc.* **2022**, *144*, 18218.
(28) Li, H.; Chavez, A. D.; Li, H.; Li, H.; Dichtel, W. R.; Bredas, J.-L. *J. Am. Chem. Soc.* **2017**, *139*, 16310.
(29) Qian, C.; Qi, Q.-Y.; Jiang, G.-F.; Cui, F.-Z.; Tian, Y.; Zhao, X. *J. Am. Chem. Soc.* **2017**, *139*, 6736.
(30) Ma, T.; Kapustin, E. A.; Yin, S. X.; Liang, L.; Zhou, Z.; Niu, J.; Li, L. H.; Wang, Y.; Su, J.; Li, J.; Wang, X.; Wang, W. D.; Wang, W.; Sun, J.; Yaghi, O. M. *Science* **2018**, *361*, 48.
(31) Vu, N.; Grunwald, M. *J. Am. Chem. Soc.* **2018**, *140*, 3306.
(32) Han, X. H.; Gong, K.; Huang, X.; Yang, J. W.; Feng, X.; Xie, J.; Wang, B. *Angew. Chem. Int. Ed.* **2022**, *61*, e202202912.
(33) Wang, S.; Zhang, Z.; Zhang, H.; Rajan, A. G.; Xu, N.; Yang, Y.; Zeng, Y.; Liu, P.; Zhang, X.; Mao, Q.; He, Y.; Zhao, J.; Li, B.-G.; Strano, M. S.; Wang, W.-J. *Matter* **2019**, *1*, 1592.
(34) Fang, Q.; Zhuang, Z.; Gu, S.; Kaspar, R. B.; Zheng, J.; Wang, J.; Qiu, S.; Yan, Y. *Nat. Commun.* **2014**, *5*, 4503.
(35) Gu, S.; Hao, R.; Chen, J. J.; Chen, X.; Liu, K.; Hussain, I.; Liu, G. Y.; Wang, Z. Q.; Gan, Q. M.; Guo, H.; Li, M. Q.; Zhang, K. L.; Lu, Z. G. *Mater. Chem. Front.* **2022**, *6*, 2545.
(36) Veldhuizen, H.; Butt, S. A.; van Leuken, A.; van der Linden, B.; Rook, W.; van der Zwaag, S.; van der Veen, M. A. *ACS Appl. Mater. Interfaces* **2023**, *15*, 29186.
(37) Guan, Q.; Zhou, L.-L.; Dong, Y.-B. *J. Am. Chem. Soc.* **2023**, *145*, 1475.
(38) Jin, E.; Asada, M.; Xu, Q.; Dalapati, S.; Addicoat, M. A.; Brady, M. A.; Xu, H.; Nakamura, T.; Heine, T.; Chen, Q.; Jiang, D. *Science* **2017**, *357*, 673.
(39) Jin, E.; Li, J.; Geng, K.; Jiang, Q.; Xu, H.; Xu, Q.; Jiang, D. *Nat. Commun.* **2018**, *9*, 4143.
(40) Jadhav, T.; Fang, Y.; Patterson, W.; Liu, C.-H.; Hamzehpoor, E.; Perepichka, D. F. *Angew. Chem. Int. Ed.* **2019**, *58*, 13753.
(41) Wei, S.; Zhang, F.; Zhang, W.; Qiang, P.; Yu, K.; Fu, X.; Wu, D.; Bi, S.; Zhang, F. *J. Am. Chem. Soc.* **2019**, *141*, 14272.
(42) Wang, Z.; Zhang, Y.; Lin, E.; Geng, S.; Wang, M.; Liu, J.; Chen, Y.; Cheng, P.; Zhang, Z. *J. Am. Chem. Soc.* **2023**, *145*, 21483.
(43) Zhang, B.; Wei, M.; Mao, H.; Pei, X.; Alshmimri, S. A.; Reimer, J. A.; Yaghi, O. M. *J. Am. Chem. Soc.* **2018**, *140*, 12715.
(44) Guan, X.; Li, H.; Ma, Y.; Xue, M.; Fang, Q.; Yan, Y.; Valtchev, V.; Qiu, S. *Nat. Chem.* **2019**, *11*, 587.
(45) Lu, M.; Zhang, M.; Liu, C. G.; Liu, J.; Shang, L. J.; Wang, M.; Chang, J. N.; Li, S. L.; Lan, Y. Q. *Angew. Chem. Int. Ed.* **2021**, *60*, 4864.
(46) Liu, J.; Yang, T.; Wang, Z.-P.; Wang, P.-L.; Feng, J.; Ding, S.-Y.; Wang, W. *J. Am. Chem. Soc.* **2020**, *142*, 20956.
(47) Lei, Z.; Chen, H.; Luo, C.; Rong, Y.; Hu, Y.; Jin, Y.; Long, R.; Yu, K.; Zhang, W. *Nat. Chem.* **2022**, *14*, 1399.
(48) Yang, Z.; Liu, J.; Li, Y.; Zhang, G.; Xing, G.; Chen, L. *Angew. Chem. Int. Ed.* **2021**, *60*, 20754.
(49) Li, X.-T.; Zou, J.; Wang, T.-H.; Ma, H.-C.; Chen, G.-J.; Dong, Y.-B. *J. Am. Chem. Soc.* **2020**, *142*, 6521.
(50) Grunenberg, L.; Savasci, G.; Terban, M. W.; Duppel, V.; Moudrakovski, I.; Etter, M.; Dinnebier, R. E.; Ochsenfeld, C.; Lotsch, B. V. *J. Am. Chem. Soc.* **2021**, *143*, 3430.
(51) Ren, X.-R.; Bai, B.; Zhang, Q.; Hao, Q.; Guo, Y.; Wan, L.-J.; Wang, D. *J. Am. Chem. Soc.* **2022**, *144*, 2488.
(52) Park, Y.; Kim, Y.; Chang, S. *Chem. Rev.* **2017**, *117*, 9247.
(53) Kumar, S. V.; Banerjee, S.; Punniyamurthy, T. *Org. Chem. Front.* **2020**, *7*, 1527.
(54) Wang, J.-C.; Kan, X.; Shang, J.-Y.; Qiao, H.; Dong, Y.-B. *J. Am. Chem. Soc.* **2020**, *142*, 16915.
(55) Wang, Z.; Zhang, X.; Liu, W.; Sun, R.; Xu, X.; Yan, Y. *Synlett* **2016**, *27*, 1563.
(56) **General procedure for the preparation of Q-COF-1:** A 10 mL Pyrex tube was charged with TAPB (42.2 mg, 0.12 mmol), DMTP (35.0 mg, 0.18 mmol), and silver trifluoromethanesulfonate (4.6 mg, 0.018 mmol). Then mesitylene (2.0 mL) was added and the mixture was sonicated for 10 min to get a homogeneous dispersion, followed by the addition of trifluoromethanesulfonic acid (3.2 µL, 0.04 mmol) and ethylene glycol (30.1 µL, 0.54 mmol). The mixture was sonicated for 10 min and sealed. The ampoule was warmed to room temperature and then kept at 120 °C without disturbance for 24 h. After being cooled to room temperature, the precipitate was collected through filtration, followed by washing three times with distilled water, EtOH, and THF, respectively. The resulting solid was dried at 120 °C for 6 h under a dynamic vacuum to afford a brown powder (77.7 mg, 98% yield).
(57) Xu, H.; Gao, J.; Jiang, D. *Nat. Chem.* **2015**, *7*, 905.
(58) Li, X.; Zhang, C.; Cai, S.; Lei, X.; Altoe, V.; Hong, F.; Urban, J. J.; Ciston, J.; Chan, E. M.; Liu, Y. *Nat. Commun.* **2018**, *9*, 2998.